MOLECULAR ECOLOGY

Molecular Ecology (2014) doi: 10.1111/mec.12968

Use of a natural hybrid zone for genomewide association mapping of craniofacial traits in the house mouse

LUISA F. PALLARES, BETTINA HARR, LESLIE M. TURNER and DIETHARD TAUTZ
Max-Planck Institute for Evolutionary Biology, Plön 24306, Germany

Abstract

The identification of the genes involved in morphological variation in nature is still a major challenge. Here, we explore a new approach: we combine 178 samples from a natural hybrid zone between two subspecies of the house mouse (*Mus musculus domesticus* and *Mus musculus musculus*), and high coverage of the genome (~ 145K SNPs) to identify loci underlying craniofacial shape variation. Due to the long history of recombination in the hybrid zone, high mapping resolution is anticipated. The combination of genomes from subspecies allows the mapping of both, variation within subspecies and inter-subspecific differences, thereby increasing the overall amount of causal genetic variation that can be detected. Skull and mandible shape were measured using 3D landmarks and geometric morphometrics. Using principal component axes as phenotypes, and a linear mixed model accounting for genetic relatedness in the mapping populations, we identified nine genomic regions associated with skull shape and 10 with mandible shape. High mapping resolution (median size of significant regions = 148 kb) enabled identification of single or few candidate genes in most cases. Some of the genes act as regulators or modifiers of signalling pathways relevant for morphological development and bone formation, including several with known craniofacial phenotypes in mice and humans. The significant associations combined explain 13% and 7% of the skull and mandible shape variation, respectively. In addition, a positive correlation was found between chromosomal length and proportion of variation explained. Our results suggest a complex genetic architecture for shape traits and support a polygenic model.

Keywords: complex traits, craniofacial shape, genetic architecture, geometric morphometrics, mandible, *Mus musculus*, skull

Received 19 June 2014; revision received 23 September 2014; accepted 3 October 2014

Introduction

Unravelling the genetic basis of organismal form remains one of the major challenges of biological research (Muller & Newman 2003; Mallarino & Abzhanov 2012). Although many efforts have been dedicated to finding genomic regions involved in morphological trait variation and adaptation, very few genes have been identified, and we are only at the beginning of understanding the developmental mechanisms generating variation in natural populations (Barrett & Hoekstra 2011; Mallarino & Abzhanov 2012). Many long-standing questions about the genetic basis of morphological adaptation remain unanswered (Orr 2005): How many loci underlie complex trait variation? What is the distribution of effect sizes of these loci? How do loci interact? Do traits have similar genetic architecture in different taxa?

Morphology can evolve rapidly between populations and species enabling adaptation to environmental changes. In particular, adult morphological traits are an important target of natural selection because they determine how an organism interacts with the environment. In this study, we focus on the adult house mouse (*Mus musculus*) craniofacial skeleton, formed by the skull and mandible.

The head is a particularly elaborated part of the vertebrate morphology, which has undergone extensive

Correspondence: Diethard Tautz, Fax: +49 4522 763 281;
E-mail: tautz@evolbio.mpg.de

© 2014 The Authors. *Molecular Ecology* Published by John Wiley & Sons Ltd.
This is an open access article under the terms of the Creative Commons Attribution-NonCommercial-NoDerivs License, which permits use and distribution in any medium, provided the original work is properly cited, the use is non-commercial and no modifications or adaptations are made.

adaptive change during the diversification of vertebrates, but is expected to be under stabilizing selection within species. Craniofacial evolution has been intensively studied due to the high prevalence of craniofacial defects in humans and because the head was a key innovation in the evolution of vertebrates (Wilkie & Morris-Kay 2001). However, there are currently few insights into the developmental processes and genetic pathways that regulate craniofacial shape formation because the complexity of craniofacial phenotypic characters cannot be adequately understood using classical genetic approaches. For example, mutagenesis screens are unlikely to detect many important variants determining morphology in the adult because they are also essential for early embryonic development. The study of gene dosage effects may provide one solution to this problem (Boell *et al.* 2013), but it requires further validation. In an alternative approach, Attanasio *et al.* (2013) have used genomic analyses and transgenic reporter gene constructs to suggest that craniofacial shape can be modified by possibly thousands of tissue-specific enhancers of developmental genes.

Most of the currently available information on mouse craniofacial features concerns the mandible; it represents a well-established model for the study of morphological shape and its underlying genetics (Atchley & Hall 1991; Klingenberg & Navarro 2012) and has a relatively simple anatomical complexity compared to the skull. Craniofacial differences between populations and subspecies of house mice have been widely studied (Gerasimov *et al.* 1990; Macholán 2006; Boell & Tautz 2011; Siahsarvie *et al.* 2012), but so far, the phenotypic differences have not been linked to the underlying gene (s). Further, it remains unclear how much variation in morphology is due to local adaptation vs. neutral drift. Results from multiple studies suggest that craniofacial morphology is under directional and/or stabilizing selection (Renaud & Auffray 2010; Boell & Tautz 2011; Siahsarvie *et al.* 2012), but the generalist diet of the house mouse makes it difficult to infer the selective pressures that might have caused the differences in shape among populations and subspecies of the *Mus musculus* group.

Genetic mapping studies—quantitative trait locus (QTL) and genomewide association studies (GWAS) — are the most common methods for identifying genes involved in complex traits. The incorporation of geometric morphometrics has enabled the application of genetic mapping approaches to craniofacial bone formation and shape determination. It has also allowed the quantification of small interindividual differences characteristic of natural populations and therefore the detection of subtle phenotypic effects (Klingenberg 2010). Using QTL mapping, many genomic regions have been associated with variation of skull and mandible shape in mice (Cheverud *et al.* 1997; Leamy *et al.* 1997, 1999, 2000; Klingenberg *et al.* 2001, 2004; Wolf *et al.* 2005). In humans, recent GWAS and candidate gene studies have identified several genes involved in non-disease-related facial variation in human populations (Boehringer *et al.* 2011; Liu *et al.* 2012; Paternoster *et al.* 2012; Claes *et al.* 2014).

Traditional QTL designs have limited mapping resolution, and the phenotypic and genomic variation in traditional laboratory strains represents a small proportion of natural variation in house mice (Yang *et al.* 2011a). In a first attempt to overcome some of these limitations, Burgio and colleagues developed interspecific congenic strains using *Mus musculus* and *Mus spretus* and mapped skull and mandible shape in mice (Burgio *et al.* 2007, 2009, 2012a,b). Currently, mouse populations with better characteristics for fine mapping are being evaluated, for example the Collaborative Cross (CTC 2004) and commercial outbred lines (Yalcin *et al.* 2010).

Genetic mapping in wild populations has been proposed as an alternative to identify loci contributing to natural trait variation (Slate *et al.* 2002; Slate 2005; Beraldi *et al.* 2007; Poissant *et al.* 2012; Schielzeth & Husby 2014). With this approach, samples with larger phenotypic and genetic variation can be studied, and good mapping resolution is predicted due to the history of recombination, (see Laurie *et al.* 2007 for specific estimates in mice), provided high-density genetic markers are available.

In this study, we use a mapping population composed of 178 males derived from a natural hybrid zone to explore the genetic architecture of skull and mandible shape in the house mouse. The same population has been used to map hybrid sterility loci in a parallel study (Turner and Harr, in press). Here, we combine 3D geometric morphometrics and association mapping for the first time to study the genetic basis of natural shape variation. This approach results in high mapping resolution—in many cases single-gene level—enabling the identification of candidate genes involved in craniofacial variation. We also show that these traits have a complex genomic architecture consistent with a polygenic model of morphological adaptation.

Materials and methods

Ethical statement

Mice were maintained and handled in accordance with FELASA guidelines and German animal welfare law (Tierschutzgesetz § 11, permit from Veterinäramt Kreis Plön: 1401-144/PLÖ-004697).

© 2014 The Authors. *Molecular Ecology* Published by John Wiley & Sons Ltd.

Mapping population

Mice were caught across the Bavarian hybrid zone and brought to the Max Planck Institute for Evolutionary Biology in Plön, Germany (Turner *et al.* 2012). Mating pairs were established using mice that were close neighbours in the wild, that is coming from the same or nearby trapping locations. In this way, the first-generation offspring was produced in a close-to-natural breeding situation. First-generation offspring were raised under identical laboratory conditions, minimizing environmentally induced shape variation. Litters were weaned at 28 days and sacrificed by CO_2 asphyxiation between 9 and 12 weeks of age. Hundred and seventy-eight male mice were included in the mapping population, including full-siblings, half-siblings and unrelated individuals. Detailed information about the sampling procedure and breeding can be found in Turner *et al.* (2012).

Shape phenotyping

Heads were scanned with a computer tomograph (micro-CT—vivaCT 40; Scanco, Bruettisellen, Switzerland), and three-dimensional cross-sections of the skull and mandible were generated with a resolution of one cross-section per 0.021 mm. Forty-eight three-dimensional landmarks were located in the skull and 14 in each hemimandible using the TINA landmarking tool (Schunke *et al.* 2012) (Table S1, Supporting information, Fig. 1). All further morphometric analyses were performed using MORPHOJ (Klingenberg 2011).

This study is focused on the symmetric component of skull and mandible shape; therefore, the raw landmark coordinates of the right and left sides were averaged. Because the skull has a pattern of object symmetry—right and left sides are connected by an internal plane of symmetry (Mardia *et al.* 2000; Klingenberg *et al.* 2002), a mirror image of the skull is generated and overlapped with the original; the average of the two images is a perfectly symmetric structure and corresponds to the symmetric component of shape (Klingenberg *et al.* 2002). The mandible has a matching symmetry pattern—right and left sides are physically independent from each other—therefore, a simple average of sides was used.

A generalized Procrustes analysis (GPA) was performed on skull and mandible averaged landmark coordinates. As the age of the mice ranged from 62 to 86 days when phenotyped, a regression of shape vs. age (days) was performed to remove shape variation due to age differences. 1.8% of the skull shape variation was explained by age (10 000 permutations, $P = 0.0002$), and 3.1% of mandible variation ($P = 0.03$). The residuals of the regression were used in a principal component analysis (PCA), and PC scores were used as phenotypes in the mapping.

Size

Centroid size (CS) is the standard measure of size in geometric morphometrics and is estimated as the square root of the sum of the squared distances of a set of landmarks from their centre of gravity or centroid (Zelditch *et al.* 2012). Using MORPHOJ, mandible CS was calculated as the average of right and left hemimandibles CS. Skull CS was calculated using all the landmarks from the right and left side (Klingenberg *et al.* 2002).

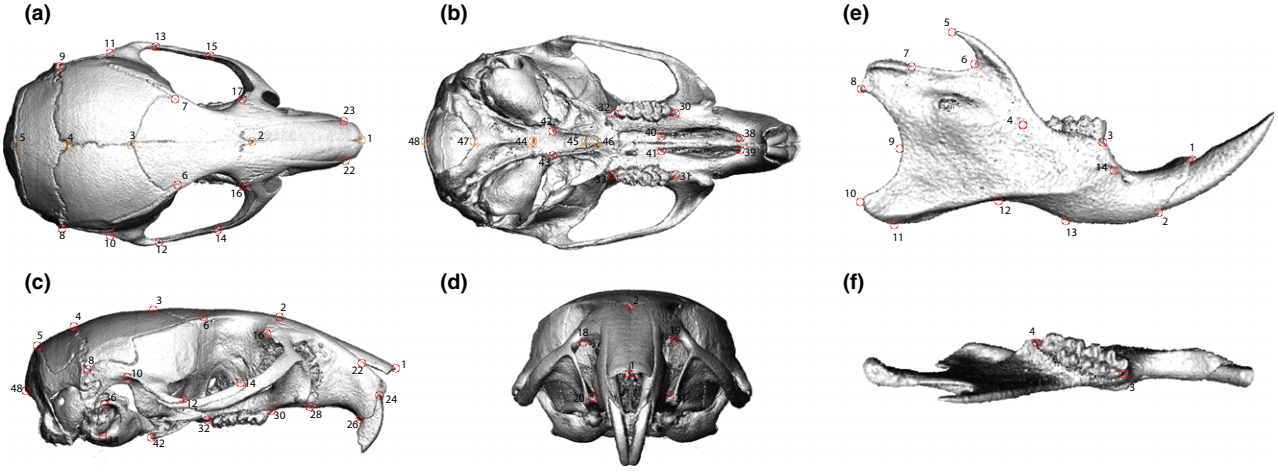

Fig. 1 Three-dimensional landmarks located in the skull and mandible. Dorsal (a), ventral (b), lateral (c) and frontal view (d) of the skull. In (a) and (b) paired landmarks (right and left) are drawn in red, midline landmarks are orange and represent the plane of symmetry. In the lateral view of the mandible (e), the landmark 4 is outside the 2D plane and its position is better represented in the dorsal view (f). See Table S1 (Supporting information) for the description of the landmarks.

© 2014 The Authors. *Molecular Ecology* Published by John Wiley & Sons Ltd.

Genotyping

DNA was extracted from liver, spleen or ear samples using salt extraction or DNeasy kits (Qiagen, Hilden, Germany). The mice were genotyped by Atlas Biolabs (Berlin, Germany) using the Mouse Diversity Genotyping Array (Affymetrix, Santa Clara, CA, USA) (Yang *et al.* 2009). Genotypes at 584 729 SNPs were called using the apt-probeset-genotype software provided by Affymetrix using standard settings. Variable intensity oligonucleotides (VINOs) were identified using the MouseDivGeno algorithm and removed from the data set (53 148 SNPs). SNPs with observed heterozygosity >0.9 (18 120 SNPs) were removed. SNPs with ≥5% missing data or minor allele frequency <5% were removed. To avoid redundancy and gain power in the mapping analysis, all SNPs in perfect linkage disequilibrium with other SNPs (LD = 1) were removed. A total of 145 378 SNPs were eventually used. The X chromosome was not analysed in this study.

Association mapping

The SNPs that passed the quality control and the PC axes that explained more than 1% of the variation in each data set (Table S2, Supporting information) were used for association mapping.

The univariate linear mixed model (LMM) implemented in genomewide efficient mixed-model association—GEMMA (Zhou & Stephens 2012) was used to perform the association mapping. This method uses a variance component model where the effect of an allele is modelled as a main effect, while population structure and relatedness among samples (estimated by a kinship matrix) are taken into account by means of variance components of random polygenic effects. The centred kinship matrix was calculated in GEMMA using all LD-pruned SNPs.

The effect size of significant SNPs was calculated in the following way (β^2 * var(x))/var(y) where var(x) is the variance of the genotype at the focal SNPs, and var (y) is the variance of the phenotype. β is reported for each SNP in the LMM output.

To estimate the genomewide parameters PVE and PGE, we used the Bayesian sparse model (BSLMM) implemented in GEMMA (Zhou *et al.* 2013). In contrast with the LMM that assumes that every genetic variant affects the phenotype, the BSLMM is flexible, allowing also the possibility that only a small proportion of the variants have some effect. As a result, BSLMM performs better for several genetic architectures and performs similar to LMM when the genetic architecture of the trait is indeed highly polygenic (Zhou *et al.* 2013). Because the architecture of the phenotypes studied here is unknown, we used BSLMM for genomewide heritability estimates. The results reported here were generated using the option –bslmm 1 (linear BSLMM) and 5 million sampling steps with 500K burn-in steps. We performed additional analyses for 10 and 50 million steps using a subsample of the data to confirm the accuracy of the Bayesian estimates (data not shown).

Permutations

The genomewide significance threshold was defined by permutation. The way in which the craniofacial phenotype is handled in this study, that is its decomposition in principal components, necessitates a high number of tests. That is, 21 tests for skull shape (20 PCs and 1 for size) and 20 for mandible shape (19 PCs and 1 for size). To account for multiple testing due to the number of SNPs and also for the number of phenotypes mapped, we performed the mapping analysis for 10 000 permuted data sets. For each repetition, all phenotypes were randomized among individuals, keeping the genotypes unaltered to preserve genetic structure. For each permutation, the best *P*-value across all phenotypes was reported and the 95% quantile of the distribution of *P*-values was used as genomewide significance threshold (Fig. S3, Supporting information). This yielded a *P*-value of 9.4×10^{-7} for skull and 8.1×10^{-7} for mandible. Bonferroni correction yields a *P*-value of 1.6×10^{-8} for skull and 1.8×10^{-8} for mandible. However, as Bonferroni correction is considered overly conservative in mapping studies, we focus the discussion on the regions identified using the permutation-based threshold.

LD analysis

Each pair of significant SNPs was tested for genotypic linkage disequilibrium (LD) by calculating the squared correlation estimator r^2. To estimate the interval associated with each significant SNP from the LD-pruned data, we report significant regions defined by the position of the most distant downstream and upstream SNP showing a minimum $r^2 = 0.8$ to the significant SNP. PLINK 1.07 (Purcell *et al.* 2007) was used for the r^2 calculations. Gene annotation for significant SNPs and regions was performed using the UCSC Genome Browser (Kent *et al.* 2002) and UCSC Annotation data (Karolchik *et al.* 2014).

In addition to studies previously reporting QTL related to craniofacial formation (cited in Table 1), we used the MGI database to search for phenotypes associated with genes in significant GWAS regions (Eppig *et al.* 2012). The QTLs reported in Leamy *et al.* (1999) do

© 2014 The Authors. *Molecular Ecology* Published by John Wiley & Sons Ltd.

Table 1 Significant SNPs associated with mandible and skull shape variation. The percentage of phenotypic variation explained by each SNP is shown

Phen	Chr	Pos	SNP	*P*-value	MAF	Gene	%var	%var total
Skull								
PC1	17	30615222	JAX00435677	3.6×10^{-7}	0.24	*Btbd9*	33.8	5.59
PC2	10	61542659	JAX00290754	4.1×10^{-7}	0.38	.	18.3	2.21
PC10	5	50372456	JAX00129855	2.8×10^{-7}	0.08	*Gpr125*	17.2	0.50
PC13	6	148560348	JAX00148139	3.8×10^{-7}	0.24	*Gm6313*	1.8	0.04
PC14	5	62659428	JAX00584067	3.2×10^{-7}	0.11	.	14.7	0.27
PC18	1	111842009	JAX00007979	9.7×10^{-7}	0.26	.	12.6	0.16
	1	113192684	JAX00262739	6.0×10^{-7}	0.30	.	13.1	0.17
	1	113521976	JAX00008104	6.9×10^{-7}	0.30	.	13.1	0.17
	1	114504925	JAX00262960	4.5×10^{-7}	0.30	.	13.4	0.17
	1	114521206	JAX00262964	7.0×10^{-7}	0.29	.	12.9	0.17
	1	114573977	JAX00262971	2.6×10^{-7}	0.29	.	13.9	0.18
	1	114667409	JAX00262998	2.4×10^{-9}	0.33	.	18.4	0.24
	1	114720894	JAX00263006	3.5×10^{-8}	0.32	.	15.7	0.20
	1	115459643	JAX00008250	3.9×10^{-7}	0.30	.	13.5	0.17
	8	90136634	JAX00164479	4.3×10^{-7}	0.20	.	13.4	0.17
	8	91911137	JAX00164612	8.7×10^{-11}	0.21	.	21.0	0.27
	8	93693782	JAX00676020	3.9×10^{-7}	0.28	.	13.5	0.17
	8	93900937	JAX00676081	3.1×10^{-7}	0.33	*Fto*	13.9	0.18
	8	93918262	JAX00676089	1.5×10^{-7}	0.33	*Fto*	14.7	0.19
	8	94057678	JAX00676176	4.8×10^{-7}	0.32	*Fto*	13.4	0.17
	8	94413228	JAX00164799	1.5×10^{-7}	0.28	.	14.4	0.19
	8	95015417	JAX00676516	9.6×10^{-7}	0.26	.	12.7	0.16
	11	51316312	JAX00027368	1.3×10^{-8}	0.12	*Col23a1*	16.6	0.21
	17	17491991	JAX0073985	2.1×10^{-8}	0.37	.	16.6	0.21
	17	17500615	JAX00432709	1.8×10^{-8}	0.36	.	16.9	0.22
	17	17500690	JAX00432710	7.0×10^{-8}	0.32	.	15.3	0.20
								12.6*
Mandible								
PC3	3	125400219	JAX00536726	9.9×10^{-7}	0.09	*Ndst4*	13.7	1.14
PC7	11	58409394	JAX00312338	9.7×10^{-7}	0.12	.	21.2	0.96
PC7	11	96437460	JAX00319199	3.4×10^{-8}	0.12	*Skap1*	16.6	0.75
PC11	15	31358406	JAX00060457	6.0×10^{-7}	0.26	.	17.6	0.50
PC11	15	31371834	JAX0039778	1.2×10^{-8}	0.23	*Ropn1 l*	19.9	0.57
PC12	15	31407662	JAX00060460	6.4×10^{-7}	0.24	*March6*	17.1	0.49
	8	52637099	JAX00668547	1.9×10^{-7}	0.09	.	15.7	0.32
PC12	17	94874936	JAX0079706	9.7×10^{-9}	0.25	.	17.6	0.36
PC13	17	94994750	JAX0079715	7.8×10^{-8}	0.38	.	15.9	0.33
	2	76287988	JAX00493638	7.7×10^{-7}	0.33	*Osbpl6*	18.7	0.37
PC15	3	106920129	JAX00111463	9.1×10^{-7}	0.46	.	12.8	0.22
PC15	3	106922140	JAX00533242	6.2×10^{-7}	0.46	.	13.1	0.23
PC16	3	106925166	JAX00533253	6.3×10^{-8}	0.47	.	15.5	0.27
	3	106930043	JAX00111464	6.8×10^{-7}	0.46	.	13.0	0.23
	16	85292313	JAX0071995	5.1×10^{-7}	0.08	.	13.1	0.18
PC18	17	4793878	JAX00430026	2.1×10^{-7}	0.36	.	20.0	0.23
								7.14*

MAF, minimum allele frequency. If the SNP falls in an intragenic region, the gene is shown. %var, variation of each PC explained by the SNP. %var total, variation of the mapping population explained by the SNP, calculated by multiplying %var of the SNP times % var of the PC (values shown in Table S2).

*Total phenotypic variation explained by the SNPs identified in this study.

not include confidence intervals; thus, we assumed overlap when our regions were within 10 Mb from peak markers (see Table 2).

Chromosomal partitioning of variance

Partitioning of the total variance among individual chromosomes was performed in the GCTA software

© 2014 The Authors. *Molecular Ecology* Published by John Wiley & Sons Ltd.

Table 2 Significant regions based on the linkage disequilibrium pattern of the significant SNPs

Nr	PC	Region	Size(Mb)	Genes	QTL
Skull					
1	PC1	chr17 : 30615222-31231411	0.616	*Glo1,Umodl1,Dnah8,Glp1r,Abcg1, Btbd9*	—
2	PC2	chr10:61467659-61617659	[0.15]	*Ass1, Neurog3*	—
3	PC10	chr5:50297456-50447456	[0.15]	*Gpr125*	—
4	PC13	chr6:148485348-148635348	[0.15]	*Gm6313*	122F[†]
5	PC14	chr5 : 62131920-62659428	0.528	*G6pd2*	—
6	PC18	chr1 : 111842009-115730660	3.889	*Dsel,Cdh7,Cdh19*	66H[†]
7		chr11:51241312-51391312	[0.15]	*Col23a1*	122D[†]
8		chr17 : 17491991-17500690	0.009	—	—
9		chr8 : 90136634-95150348	5.014	*Zfp423,Cnep1r1,Heatr3,Papd5,Adcy7, Brd7,**Nkd1**,Snx20,Nod2,**Cyld**,Sall1, Tox3,**Chd9**, **Rbl2**,Aktip,**Rpgrip1 l**,Fto,**Irx3**,**Irx5***	122F[†]
Mandible					
10	PC3	chr3:125325219-125475219	[0.15]	*Ndst4*	—
11	PC7	chr11:58334394-58484394	[0.15]	*Olfr224, 322-325, 328, 330, 2210407C18Rik,Trim58*	122D[‡]
12		chr11:96362460-96512460	[0.15]	*Skap1*	SH11.2[§]
13	PC11	chr15 : 31319098-31494802	0.176	*Ropn1 l, March6*	SH15.1[§]
14	PC12	chr17 : 94874936-94994750	0.120	—	—
15		chr8:52562099-52712099	[0.15]	—	—
16	PC13	chr2 : 76284649-76329794	0.045	*Osbpl6*	—
17	PC15	chr3 : 106920129-106997029	0.077	*Kcna10*	SH3.2[§]
18	PC16	chr16:85217313-85367313	[0.15]	—	136E[‡]
19	PC18	chr17 : 4741573-4844025	0.102	—	6C[‡]

Regions were defined using a correlation threshold with neighbouring SNPs of $r2 = 0.8$ (see methods). Only protein-coding genes are shown, based on the UCSC annotation database. The parentheses indicate regions where the focal SNP did not show linkage to other SNPs, and therefore, the region was expanded to the median region size of 0.15 Mb (see Results). Overlap with previous QTL reported for shape is shown,

[†]Burgio *et al.* 2009;

[‡]Burgio *et al.* 2012a;

[§]Leamy *et al.* 2008.

Genes in bold in region 9 are known to display craniofacial phenotypes when mutant (see text).

(Yang *et al.* 2011b). GCTA performs a restricted maximum-likelihood analysis to calculate the variance explained by each chromosome while controlling for the effect of the others, this means that relatedness and population structure are accounted for (option –reml –mgrm). Due to the small number of mice used in this study, it was not possible to fit all 19 autosomes at the same time. Individual analyses were run for each chromosome including the first 10 principal components derived from the kinship matrix as covariates (option –reml –grm –qcovar). Resulting per-chromosome estimates are inflated due to relatedness among individuals; hence, the sum of all chromosomes effects exceeds the heritability estimates for each phenotype. However, because overestimation is uniformly spread across the genome (Yang *et al.* 2011c), the relative effects of chromosome are informative even though absolute estimates are error-prone. We calculated the relative contribution of each chromosome by dividing individual values over the total variation explained.

Regression of shape on genetic admixture

To explore the pattern of change in craniofacial morphology through the hybrid zone, a multivariate regression was performed between skull and mandible shape and hybrid index (% *M. m. musculus* ancestry, Turner *et al.* (2012)). Shape vectors were obtained using MORPHOJ following the generalized Procrustes fit, and multivariate regression was performed using MORPHOJ.

Eleven wild-caught mice from the *M. m. musculus* extreme of the hybrid zone and 19 from the *M. m. domesticus* side were also included in the regression. These mice were not environmentally controlled; therefore, they differ in age, sex and other environmental factors.

Morphological differences between house mouse subspecies

Ten mice from the Cologne/Bonn region in Germany (*M. m. domesticus*) and 15 from Kazakhstan (*M. m. musculus*) were used to illustrate the craniofacial shape

© 2014 The Authors. *Molecular Ecology* Published by John Wiley & Sons Ltd.

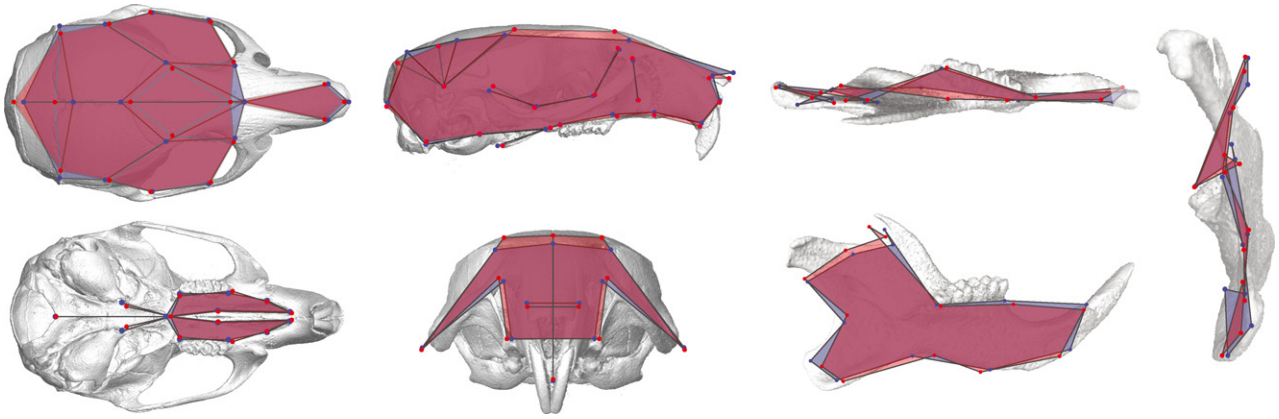

Fig. 2 Shape differences between the two subspecies of *Mus musculus* that encounter each other in the European mouse hybrid zone, *Mus musculus musculus* (eastern European) and *Mus musculus domesticus* (western European). Blue, mean shape of *M. m. domesticus*. Red, mean shape of *M. m. musculus*. Differences are scaled by 2×. Wild-derived mice from the German region of Cologne/Bonn were used to represent the *M. m. domesticus* subspecies, and mice from Kazakhstan to represent the *M. m. musculus* subspecies. The underlying skull and mandible images are provided for orientation and do not directly represent the landmarks.

differences between the two subspecies of mice (Fig. 2). The mice were sacrificed by CO_2 asphyxiation at nonmatched ages. These mice are part of the wild colonies kept in the Max Plank Institute for Evolutionary Biology in Plön, Germany. Phenotypes were measured as described above for hybrid mice, with a slightly different set of landmarks (44 for the skull and 13 for the mandible—see Fig. 2). Differences between the mean shapes of the two subspecies were calculated using the discriminant function implemented using MORPHOJ.

Results

Phenotypic variation

M. m. musculus and *M. m. domesticus* show subtle differences in skull and mandible shape; however, these differences can be precisely quantified using geometric morphometrics. *M. m. domesticus* is characterized by a relatively flat skull vault and a broader back of the cranium. Its frontal bone is longer and wider, making the middle of the cranium more robust compared to *M. m. musculus*. The ascending ramus of the mandible is more robust and compact in *M. m. domesticus*. The coronoid process is much more pronounced in *M. m. musculus*, and the angle between the condyle and the angular process is wider. From a posterior view, it is evident that the buccal–lingual contrast is more marked in *M. m. domesticus*, with *M. m. musculus* having a relatively straight disposition (Fig. 2).

The animals used in this study were first-generation offspring of mice captured in a natural hybrid zone in Bavaria (Turner *et al.* 2012). Skull morphology measurements were based on computer tomography scans and 3D landmarks (Fig. 1). Regression of shape vectors on individual measures of genetic admixture (see Methods) showed that most hybrid phenotypes are intermediate between pure subspecies' phenotypes (inferred from individuals with >80% genomic make-up from one subspecies; Fig. S1, Supporting information). These results suggest that transgressive phenotypes, that is hybrid phenotypes outside the range of the pure subspecies, are not of special relevance for the craniofacial morphology in this population. Inclusion of wild-caught, not environmentally controlled, mice from the extremes of the hybrid zone into the regression did not alter the pattern substantially (Fig. S1, Supporting information), showing that indeed, the first-generation laboratory-bred hybrids represent the full range of phenotypic transition between the subspecies.

Genetic architecture

We analysed skull and mandible separately. Right and left sides of the structures were averaged and corrected for age differences using a multivariate regression of shape vs. age. On each of the data sets, we performed a GPA of the raw landmark coordinates, followed by a PCA to reduce the dimensionality of the data and make it suitable for the association analysis.

All PC axes explaining at least 1% of the total phenotypic variation were included in the mapping: 20 axes for skull explaining 86% of the total observed shape variation and 18 axes for mandible explaining 92% of the variation (Table S2, Supporting information). The PC scores were used as individual phenotypes. The complex genetic relatedness of the mapping population was accounted for using the LMM implemented in GEMMA (Fig. S4, Supporting information).

© 2014 The Authors. *Molecular Ecology* Published by John Wiley & Sons Ltd.

No significant genetic associations were found for skull or mandible size (CS measurement).

To estimate to which extent the shape changes associated with each PC axis have a genetic basis, we calculated the 'chip heritability' of each PC. The 'chip heritability' -from now on PVE, to match the GEMMA output- is the percent of phenotypic variation explained by all the SNPs used in the mapping. We find a strong genetic signal in most of the PCs, with 25 of the 38 PCs having PVE values above 50% (Table S2, Supporting information). The total PVE estimate for skull and mandible shape suggests that $\sim$ 64% of the phenotypic variation has a genetic basis. For size, the estimate reaches $\sim$72% (Table S2, Supporting information).

Most of the chip heritability can be attributed to SNPs of small effect, also known as polygenic effect. However, there are SNPs with effect size above the polygenic level. The percentage of phenotypic variation explained by the latter (from now on PGE) was estimated. ~30–37% of shape and size variation is explained by such 'large-effect' SNPs (Table S2, Supporting information), leaving a large proportion of the variation to be explained by loci with small effect. PGE values, however, should not be overinterpreted due to the relatively high error estimates (Table S2, Supporting information).

We calculated the proportion of variation explained by each chromosome and tested for a correlation between this parameter and chromosomal length. A positive correlation was found for mandible and skull shape; that is, the longer the chromosome, the more variation it explains (Fig. 3), suggesting a more or less random distribution of major and minor effect loci across the chromosomes.

Genomic regions associated with shape

We identified significant associations for six of the 20 PC axes included for skull and for 8 of the 18 PC axes for mandible (see Table S2, Supporting information). The skull and mandible shape traits that showed association with genetic variant(s) are depicted in Figs S5 and S6 (Supporting information). Following the genomewide significance threshold of $P < 8 \times 10^{-7}$ defined through permutations (see Methods and Fig. S3, Supporting information), a total of 27 SNPs showed significant associations with skull and 16 SNPs with mandible shape variation (Table 1, Fig. 4). 28% of these SNPs fall inside genic regions.

Together, the group of SNPs identified in this study explain 13% of the total variation in skull shape in the mapping population and 7% of the mandible variation (Table 1). The biggest effect is caused by the SNP associated with skull PC1, which is the major axis of shape variation in the hybrid population. The distribution of effect sizes is shown in Fig. 5.

We tested for long-range LD between pairs of significant SNPs. We did not find any significant linkage between physically distant SNPs, suggesting the associations found in this population are not confounded by diffuse or long-range LD. LD blocks were calculated for each focal SNP, first using $r^2 \geq 0.2$, with the purpose of exploring the maximum block size showing any linkage. The median size was 1.8 Mb (max = 1.99 Mb, min = 0.97 Mb). Using a more meaningful threshold of $r^2 \geq 0.8$, the median size of the regions was 0.15 Mb.

After grouping the SNPs based on LD ($r^2 \geq 0.8$), a total of 19 genomic regions associated with craniofacial traits were defined (Table 2). The phenotypic effect of the genotypes for the significant regions is shown in Fig. S2 (Supporting information). For all SNPs, phenotypic means for heterozygous individuals were intermediate between the means of the homozygous classes, suggesting most effects are additive.

Nine genomic regions were associated with skull shape. Regions 6 and 9 contain some SNPs that are not in strong linkage, but are still relatively close together

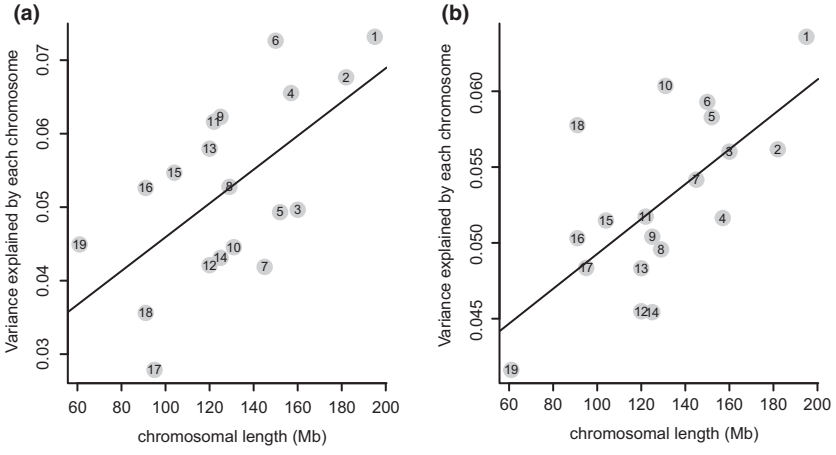

Fig. 3 Correlation between variance explained and chromosome length for skull (a) and mandible (b). The units of variance explained by chromosome are arbitrary and were adjusted to add up to one. Numbers in the circles represent chromosome number. $R^2 = 0.33$, $P = 0.005$ for skull, and $R^2 = 0.40$, $P = 0.002$ for mandible.

© 2014 The Authors. *Molecular Ecology* Published by John Wiley & Sons Ltd.

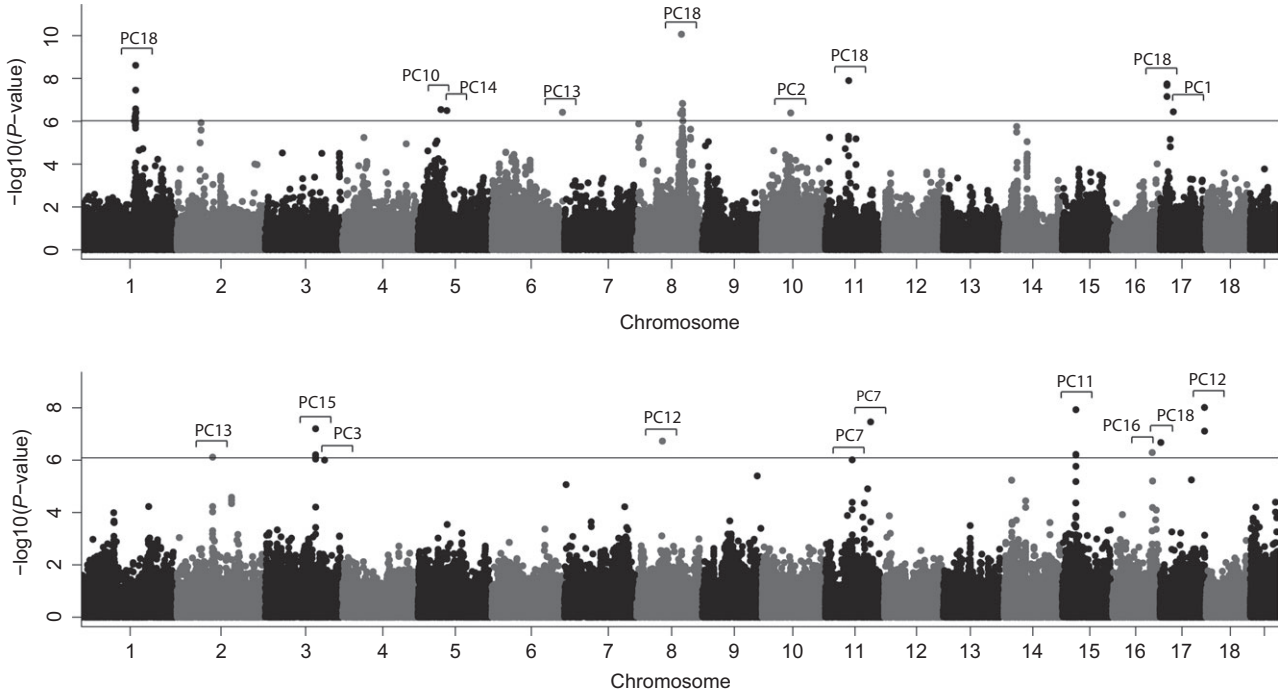

Fig. 4 Manhattan plots showing the significant associations found for skull shape (top) and mandible shape (bottom). The phenotype (PC axis) associated with each SNP is shown. The blue line indicates the significant threshold used in this study: 9.4×10^{-7} for skull and 8.1×10^{-7} for mandible (see Methods). Only one SNP per perfect linkage group (LD = 1) is shown (see methods).

(~0.5–2 Mb apart) and therefore were combined into single regions. Mandible shape was associated with 10 genomic regions. The median size of the regions was 148 kb (min = 8.7 kb, max = 5013 kb). For several significant SNPs, there were no highly linked SNPs in the data set; hence, the inferred significant intervals are 1 bp in length. We did not include these intervals in median estimates of mapping resolution. However, when evaluating potential candidate genes, we included 150-kb intervals (median for other regions) around each of these SNPs.

The significant regions identified in this study overlap with previous QTL studies of skull and mandible shape in mice. For the sake of precision, we did not include studies for which QTL intervals were reported only in cM, but only those with precise intervals reported in bp. Four of the nine regions associated with skull shape overlap with the results of Burgio *et al.* (2009), who used interspecific recombinant congenic strains (IRCS) between C57BL/6 and *Mus spretus* to explore the genetic basis of skull shape. Six of the 10 regions associated with mandible shape overlap with regions in Burgio *et al.* (2012a) and/or with Leamy *et al.* (2008), who used IRCS and a F3 SM/J—LG/J crosses to explore mandible variation, respectively.

Twelve of the significant SNPs fall in intronic regions of 10 genes (Table 1). Among them is *Ndst4*, associated with PC3 of the mandible, which codes for a heparan sulfotransferase, a family of proteins involved in craniofacial formation through the modulation of BMP, Wnt, Shh and FGF signalling, for example *Ndst1* (Hu *et al.* 2007; Pallerla *et al.* 2007). The specific role of *Ndst4* in craniofacial formation is not yet known.

Several interesting candidate genes are found inside the significant regions (Table 2). *Glo1* (glyoxalase 1, region 1, skull PC1) is involved in osteoclastogenesis, stimulating the maturation of osteoclasts (Kawatani *et al.* 2008). Two members of the cadherin family, *Cdh7* and *Cdh19*, are found in region 6. This family is well known for its function in bone formation through the mediation of cell–cell interactions (Hay *et al.* 2009; Marie & Hay 2013).

Region 9 comprises several genes, including seven with well-known roles in bone formation. *Irx3* and *Irx5* are part of the Iroquois homeobox gene family of transcription regulators. *Irx5* modulates craniofacial development through regulation of neural crest cells (NCC) migration and is co-expressed with *Irx3*, and they both interact at the protein level (Bonnard *et al.* 2012). These genes are regulated by *BMP2* and *BMP4* and are expressed in NCC, embryonic maxillary mesenchymal and others. Compound knockout mice have craniofacial defects.

Another interesting candidate gene in region 9 is *Nkd1*, which regulates the wnt/β-catenin signalling

© 2014 The Authors. *Molecular Ecology* Published by John Wiley & Sons Ltd.

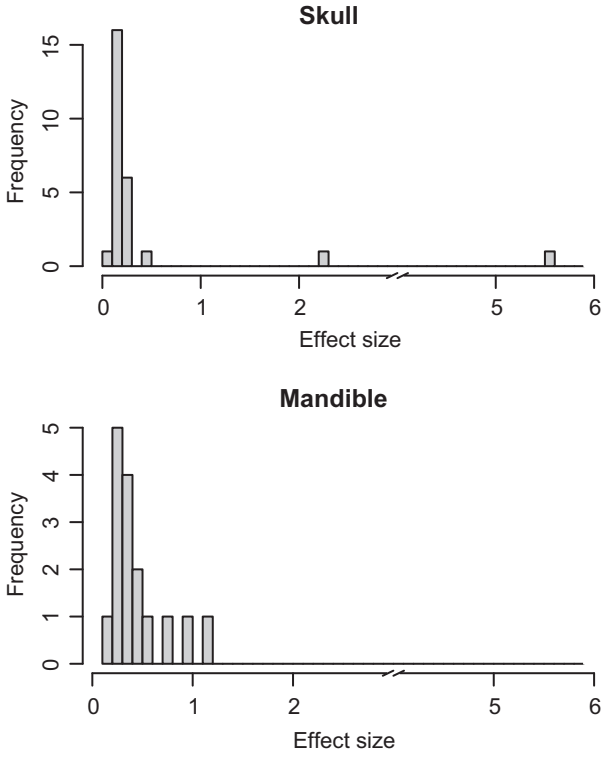

Fig. 5 Distribution of the effect sizes for mandible and skull shape. Effect size is the percentage of the total phenotypic variation explained by the focal SNP. Note the broken scale to represent one large value in skull.

pathway. *Nkd1* knockouts show a subtle craniofacial phenotype that becomes significant when *Nkd2* is knocked out at the same time (Zhang *et al.* 2007). *Rbl2* shows a similar effect; it has no phenotype, but when knocked out together with *Rbl1*, mice show severe cranium deformations due to abnormal endochondral ossification (Cobrinik *et al.* 1996). *Cyld*, a de-ubiquitinating enzyme, regulates the maturation of osteoclasts (Jin *et al.* 2008). *Rpgrip1 l* is involved in cilia-mediated *Shh* signalling, and knockout mice have craniofacial deformations (Delous *et al.* 2007; Vierkotten *et al.* 2007). And lastly, *Chd9*, a chromatin-remodelling protein, may be involved in transcriptional regulation of osteoprogenitor cells due to its ability to bind to the regulatory region of critical promoters for osteoblastogenesis including *Bmp4*, *OC* and others (Shur *et al.* 2006).

The gene *Zfp423*, a transcription factor involved in cerebellar and olfactory development, is also found in this region (Alcaraz *et al.* 2011). Although its role in bone morphogenesis has not been shown yet, it modulates the action of BMP target genes (Masserdotti *et al.* 2010), and knockout mice have a small nasal cavity (Cheng & Reed 2007).

Discussion

Natural hybrid zone

The main logistical challenge of mapping in natural populations of mice is obtaining samples of sufficient size, estimated to be thousands of individuals for quantitative traits similar to human studies (Laurie *et al.* 2007; Flint & Eskin 2012). However, mapping in naturally admixed populations from hybrid zones (between species or subspecies) has benefits that may enable mapping with smaller sample sizes (Rieseberg & Buerkle 2002; Slate 2005; Buerkle & Lexer 2008). Phenotypic variation in hybrid zones includes both intra-subspecific polymorphism and inter-subspecific differences. Because many of the latter causative genetic variants are expected to be fixed within their respective subspecies, they may occur at higher frequency in the hybrid zone than segregating alleles contributing to variation within populations. Further, hybrid zones represent hundreds of generations of intercrossing between differentiated lineages, and therefore, mapping resolution is expected to be high relative to laboratory crosses. Our genomewide association mapping in the house mouse hybrid zone is thus comparable to mapping in recombinant inbred lines, where a relatively small number of individuals also can yield reliable results (Flint & Eskin 2012).

Hybrid zones that have formed recently or those with large amounts of gene flow from source populations may be less suitable for such association studies. For example, a large influx of pure subspecies chromosomes into the hybrid zone could lead to long-range associations between genomic regions from different chromosomes (Rieseberg & Buerkle 2002; Teeter *et al.* 2008). We tested for this potentially confounding effect by measuring LD between the significant SNPs. No association between significant SNPs was found, improving our confidence that the identified regions are not artefacts of unusual population structure.

The phenotype of interest in this study, morphological shape, is known to be susceptible to environmental influences. Laboratory studies have shown that diet and age can have plastic effects on the shape of the mouse mandible (Renaud *et al.* 2010; Boell & Tautz 2011). However, genetic effects are usually stronger than environmental effects (Boell & Tautz 2011). Here, we have reduced the influence of environmental effects by breeding wild-caught mice from the hybrid zone for one generation under laboratory conditions and using the first-generation offspring of the same gender as mapping population. We have furthermore corrected for any effect on shape of the small variation in age (1 month) among individuals.

© 2014 The Authors. *Molecular Ecology* Published by John Wiley & Sons Ltd.

To avoid spurious associations due to relatedness or population structure, we used a mixed-model approach implemented in GEMMA (Zhou & Stephens 2012), which corrects for genetic structure using a kinship matrix derived from the data. This approach has not been tested previously in hybrid populations; however, it seems to have corrected accurately for structure in our sample (Fig. S4, Supporting information).

Genetic architecture of craniofacial shape variation

The significant loci identified in this study were associated with a wide range of PCs, from a PC axis explaining a large amount of the total variation (i.e. PC1 and PC2 in skull and PC3 in mandible) to PCs explaining as little as ~1% of the variation. This implies that shape changes representing a small amount of the total variation in the population can be explained, at least to some extent, by genetic variants. This is striking, as it is customary to assume that PCs with low variation do not contain much biological information. However, compiling data from two QTL studies for mandible shape in mouse, Boell (2013) found a similar pattern, PCs explaining diverse amounts of variation were associated with QTLs. Moreover, our PVE estimates per PC show that most of them have high chip heritability values (see Table S2, Supporting information), including some with values above 90%. However, the estimation error is high in some cases, probably due to relatively small sample size (Yang *et al.* 2010), and therefore, these values should be interpreted with caution.

We identified nine genomic regions explaining ~13% of the variation in skull and 10 explaining ~7% of mandible variation. Based on the PVE estimates, the markers included in this study can explain 64% of total craniofacial variation. We controlled for environmental effects such as age, sex, diet and age at weaning; we expect that heritability of these traits is lower in nature, where environmental factors play an important role. Nevertheless, the PVE indicates that there are more genetic variants that were not detected, possibly due to small effect sizes. These results are consistent with a polygenic model of morphological shape, that is, many loci of small effect are responsible for between species variation.

We estimated the contribution of individual chromosomes to phenotypic variation, following Yang *et al.* (2011c) (Fig. 3). Based on the PVE and PGE estimates, we expect many loci with small effect to affect shape variation. As expected, there is a positive correlation between chromosome length and variation explained. This result provides additional evidence that many genes of small effect underlie shape variation.

The effect sizes of individual SNPs estimated in this study range from 0.1% to 5%. With the exception of the single SNP (Region 1) explaining ~5%, the distribution of effect sizes is within the range expected for mouse craniofacial shape variation (N. Navarro, personal communication). A similar range of effects was reported for loci affecting human facial traits (Claes *et al.* 2014) although loci with very small effects (<1%) were not detected in that study, probably because a specific set of candidate genes with known roles in craniofacial development was interrogated.

We encourage caution when interpreting estimates of effect sizes; values are probably overestimated due to the Beavis effect (Beavis 1998). Recently, Slate (2013) showed that all QTL studies performed in wild and outbred populations have overestimated the QTL effect sizes, giving the false impression that most traits are oligogenic.

On the basis of heritability estimates and comparison with previous QTL studies of skull and mandible shape (Klingenberg *et al.* (2004)—33 mandible QTLs, Leamy *et al.* (2008)—36 mandible QTLs, Leamy *et al.* (1999)—26 skull QTLs), we expect the number of loci reported here is an underestimate of the total number underlying craniofacial shape variation in nature.

Candidate genes

Some of the genomic regions identified here overlap with previously identified QTL for craniofacial phenotypes (Table 2). However, because no previous studies have reached gene-level resolution, it is unclear whether overlap with previous QTL studies is due to the same underlying causative genes.

The inferences on the identified candidate genes are mostly derived from knockout studies. However, such studies have limited power to reveal functions of regulatory or signalling genes involved in multiple developmental processes, because many processes involved in bone shape specification occur late in development. Moreover, most standard phenotyping approaches of knockout mice do not involve the refined morphometric procedures that we have applied here and phenotypes might therefore have been missed. For example, a pilot study showed that subtle morphological phenotypes can be detected in mice heterozygous for mutations in developmental regulator genes (Boell *et al.* 2013).

Nevertheless, some genes identified here have craniofacial and skeletal phenotypes, representing strong candidates. Future studies, using more subtle approaches to manipulate these and other candidate genes derived from GWAS studies, will show whether these indeed affect the anticipated phenotype.

Craniofacial morphology evolves rapidly between populations and species. Much of this evolution appears to reflect responses to the species' ecology (Boell & Tautz 2011). On the other hand, many genes influencing shape

© 2014 The Authors. *Molecular Ecology* Published by John Wiley & Sons Ltd.

variation are highly conserved, implying that the pathways involved in craniofacial shape development may be generally conserved. Variation and rapid divergence in morphology, then, probably arises from finer details of developmental processes. The results of Attanasio *et al.* (2013) suggest that regulation by distant enhancers plays an important role in determining shape development. This may explain why some significant intervals identified here are in regions without annotated genes (Table 1). In addition, for intervals with candidate genes, causative mutations affecting the regulation of these or other genes should be considered in addition to mutations in coding sequence.

Region 9 encompasses a cluster of genes with known craniofacial phenotypes or roles in regulatory signalling pathways for craniofacial development. Part of this region, including the genes *Aktip*, *Rpgrip1 l*, *Fto*, *Irx3*, *Irx5*, and *Irx6* is deleted in *Fused toes* mice (Peters *et al.* 2002), which are characterized by neural tube defects, left–right asymmetry, polydactyly and craniofacial defects, among other phenotypes. Experiments aimed at identifying the causative gene for this region have revealed that at least three of the genes (*Rpgrip1 l*, *Irx3*, *Irx5*) have individual effects on craniofacial phenotypes (Bonnard *et al.* 2012). In humans, a duplication including homologues of mouse genes in region 9 (*Rbl2*, *Aktip*, *Rpgrip1 l*, *Fto*) is associated with dysmorphic faces and other phenotypes (Stratakis *et al.* 2000). Region 9 contains three additional genes with well-known roles in craniofacial development (*Nkd1*, *Cyld*, *Chd9*) and the transcription factor *Zfp423*, a known regulator of BMP signalling with a complex role in brain morphogenesis that might also affect the skull. Taken together, this evidence indicates region 9 may represent a hotspot of genes involved in craniofacial bone formation and shape variation.

The overlap with previous QTL studies (see Results) shows that the approach taken here offers the possibility of resolving previously mapped regions, but also enables the discovery of new variants that are probably not variable among classical laboratory strains.

Conclusions

This study has achieved three main goals. First, we identified loci involved in craniofacial shape variation in wild mice. Several of these genes are strong candidates for future investigations of developmental pathways for craniofacial morphology. Moreover, because we focused on naturally occurring variation in a hybrid population between emerging species, these loci may also elucidate the evolutionary dynamics of shape diversification.

Second, we find support for a polygenic architecture underlying craniofacial morphology in mice and generate the first estimates of craniofacial shape heritability based on a dense SNP coverage of the genome.

Third, we have shown the feasibility of using natural hybrid zones for exploring the genetic basis of complex traits. In a parallel study, the same mapping population was successfully used to map genes and gene interactions involved in reproductive isolation (Turner and Harr, in press). Natural hybrid zones exist for many animal and plant species and have long been recognized as a potentially powerful mapping resource. Our results encourage the use of such natural systems for future mapping studies.

Acknowledgements

We thank the mouse team in Plön for raising the mice, Anja Schunke for advice on the digitisation of 3D landmarks, Rafik Neme for bioinformatics assistance and Jun Wang and John Baines for giving us access to wild-caught mice from the extremes of the hybrid zone. We also thank Xiang Zhou and Peter Carbonetto for help with GEMMA. LFP is a member of the International Max Planck Research School (IMPRS) for Evolutionary Biology.

References

Alcaraz WA, Chen E, Valdes P *et al.* (2011) Modifier genes and non-genetic factors reshape anatomical deficits in Zfp423-deficient mice. *Human Molecular Genetics*, **20**, 3822–3830.

Atchley WR, Hall BK (1991) A model for development and evolution of complex morphological structures. *Biological Reviews*, **66**, 101–157.

Attanasio C, Nord AS, Zhu Y *et al.* (2013) Fine tuning of craniofacial morphology by distant-acting enhancers. *Science* **342**, 1241006.

Barrett RD, Hoekstra HE (2011) Molecular spandrels: tests of adaptation at the genetic level. *Nature Reviews Genetics*, **12**, 767–780.

Beavis WD (1998) QTL analyses: power, precision, and accuracy. In: *Molecular Analysis of Complex Traits* (ed. Paterson A), pp. 145–161. CRC Press, Boca Raton, FL.

Beraldi D, McRae AF, Gratten J, Slate J, Visscher PM, Pemberton JM (2007) Mapping quantitative trait loci underlying fitness-related traits in a free-living sheep population. *Evolution*, **61**, 1403–1416.

Boehringer S, van der Lijn F, Liu F *et al.* (2011) Genetic determination of human facial morphology: links between cleft-lips and normal variation. *European Journal of Human Genetics*, **19**, 1192–1197.

Boell L (2013) Lines of least resistance and genetic architecture of house mouse (*Mus musculus*) mandible shape. *Evolution & Development*, **15**, 197–204.

Boell L, Tautz D (2011) Micro-evolutionary divergence patterns of mandible shapes in wild house mouse (*Mus musculus*) populations. *BMC Evolutionary Biology*, **11**, 306.

Boell L, Pallares LF, Brodski C *et al.* (2013) Exploring the effects of gene dosage on mandible shape in mice as a model for studying the genetic basis of natural variation. *Development Genes and Evolution* **223**, 279–287.

© 2014 The Authors. *Molecular Ecology* Published by John Wiley & Sons Ltd.

Bonnard C, Strobl AC, Shboul M *et al.* (2012) Mutations in IRX5 impair craniofacial development and germ cell migration via SDF1. *Nature Genetics*, **44**, 709–713.

Buerkle CA, Lexer C (2008) Admixture as the basis for genetic mapping. *Trends in Ecology & Evolution*, **23**, 686–694.

Burgio G, Szatanik M, Guenet JL, Arnau MR, Panthier JJ, Montagutelli X (2007) Interspecific recombinant congenic strains between C57BL/6 and mice of the *Mus spretus* species: a powerful tool to dissect genetic control of complex traits. *Genetics*, **177**, 2321–2333.

Burgio G, Baylac M, Heyer E, Montagutelli X (2009) Genetic analysis of skull shape variation and morphological integration in the mouse using interspecific recombinant congenic strains between C57BL/6 and mice of the *Mus spretus* species. *Evolution*, **63**, 2668–2686.

Burgio G, Baylac M, Heyer E, Montagutelli X (2012a) Exploration of the genetic organization of morphological modularity on the mouse mandible using a set of interspecific recombinant congenic strains between C57BL/6 and mice of the *Mus spretus* species. *G3* **2**, 1257–1268.

Burgio G, Baylac M, Heyer E, Montagutelli X (2012b) Nasal bone shape is under complex epistatic genetic control in mouse interspecific recombinant congenic strains. *PLoS One* **7**, e37721.

Cheng LE, Reed RR (2007) Zfp423/OAZ participates in a developmental switch during olfactory neurogenesis. *Neuron*, **54**, 547–557.

Cheverud JM, Routman EJ, Irschick DJ (1997) Pleiotropic effects of individual gene loci on mandibular morphology. *Evolution*, **51**, 2006–2016.

Claes P, Liberton DK, Daniels K *et al.* (2014) Modeling 3D facial shape from DNA. *PLoS Genetics*, **10**, e1004224.

Cobrinik D, Lee M-H, Hannon G *et al.* (1996) Shared role of the pRB-related p130 and p107 proteins in limb development. *Genes & Development*, **10**, 1633–1644.

CTC (2004) The Collaborative Cross, a community resource for the genetic analysis of complex traits. *Nature Genetics*, **36**, 1133–1137.

Delous M, Baala L, Salomon R *et al.* (2007) The ciliary gene RPGRIP1L is mutated in cerebello-oculo-renal syndrome (Joubert syndrome type B) and Meckel syndrome. *Nature Genetics*, **39**, 875–881.

Eppig JT, Blake JA, Bult CJ, Kadin JA, Richardson JE; Mouse Genome Database Group (2012) The Mouse Genome Database (MGD): comprehensive resource for genetics and genomics of the laboratory mouse. *Nucleic Acids Research*, **40**, D881–D886.

Flint J, Eskin E (2012) Genome-wide association studies in mice. *Nature Reviews Genetics*, **13**, 807–817.

Gerasimov S, Nikolov H, Mihailova V, Auffray J-C, Bonhomme F (1990) Morphometric stepwise discriminant analysis of the five genetically determined European taxa of the genus *Mus*. *Biological Journal of the Linnean Society*, **41**, 47–64.

Hay E, Laplantine E, Geoffroy V *et al.* (2009) N-cadherin interacts with axin and LRP5 to negatively regulate Wnt/beta-catenin signaling, osteoblast function, and bone formation. *Molecular and Cellular Biology*, **29**, 953–964.

Hu Z, Yu M, Hu G (2007) NDST-1 modulates BMPR and PTHrP signaling during endochondral bone formation in a gene knockout model. *Bone*, **40**, 1462–1474.

Jin W, Chang M, Paul EM *et al.* (2008) Deubiquitinating enzyme CYLD negatively regulates RANK signaling and osteoclastogenesis in mice. *The Journal of Clinical Investigation*, **118**, 1858–1866.

Karolchik D, Barber GP, Casper J *et al.* (2014) The UCSC Genome Browser database: 2014 update. *Nucleic Acids Research*, **42**, D764–770.

Kawatani M, Okumura H, Honda K *et al.* (2008) The identification of an osteoclastogenesis inhibitor through the inhibition of glyoxalase I. *Proceedings of the National Academy of Sciences of the United States of America*, **105**, 11691–11696.

Kent WJ, Sugnet CW, Furey TS *et al.* (2002) The human genome browser at UCSC. *Genome Research*, **12**, 996–1006.

Klingenberg CP (2010) Evolution and development of shape: integrating quantitative approaches. *Nature Reviews Genetics*, **11**, 623–635.

Klingenberg CP (2011) MorphoJ: an integrated software package for geometric morphometrics. *Molecular Ecology Resources*, **11**, 353–357.

Klingenberg CP, Navarro N (2012) Development of the mouse mandible. In: *Evolution of the House Mouse* (eds Macholán M, Baird SJE, Munclinger P, Pialek J), pp. 135–149. Cambridge University Press, Cambridge.

Klingenberg CP, Leamy LJ, Routman EJ, Cheverud JM (2001) Genetic architecture of mandible shape in mice: effects of quantitative trait loci analyzed by geometric morphometrics. *Genetics*, **157**, 785–802.

Klingenberg CP, Barluenga M, Meyer A (2002) Shape analysis of symmetric structures: quantifying variation among individuals and asymmetry. *Evolution*, **56**, 1909–1920.

Klingenberg CP, Leamy LJ, Cheverud JM (2004) Integration and modularity of quantitative trait locus effects on geometric shape in the mouse mandible. *Genetics*, **166**, 1909–1921.

Laurie CC, Nickerson DA, Anderson AD *et al.* (2007) Linkage disequilibrium in wild mice. *PLoS Genetics*, **3**, 1487–1495.

Leamy LJ, Routman EJ, Cheverud JM (1997) A search for quantitative trait loci affecting asymmetry of mandibular characters in mice. *Evolution*, **51**, 957–969.

Leamy LJ, Routman EJ, Cheverud JM (1999) Quantitative trait loci for early- and late-development skull characters in mice: a test of the genetic independence model of morphological integration. *The American Naturalist*, **153**, 201–214.

Leamy LJ, Pomp D, Eisen EJ, Cheverud JM (2000) Quantitative trait loci for directional but not fluctuating asymmetry of mandible characters in mice. *Genetics Research (Camb)*, **76**, 27–40.

Leamy LJ, Klingenberg CP, Sherratt E, Wolf JB, Cheverud JM (2008) A search for quantitative trait loci exhibiting imprinting effects on mouse mandible size and shape. *Heredity (Edinb)*, **101**, 518–526.

Liu F, van der Lijn F, Schurmann C *et al.* (2012) A genome-wide association study identifies five loci influencing facial morphology in Europeans. *PLoS Genetics*, **8**, e1002932.

Macholán M (2006) A geometric morphometric analysis of the shape of the first upper molar in mice of the genus *Mus* (Muridae, Rodentia). *Journal of Zoology*, **270**, 672–681.

Mallarino R, Abzhanov A (2012) Paths less traveled: evo-devo approaches to investigating animal morphological evolution. *Annual Review of Cell and Developmental Biology*, **28**, 743–763.

Mardia KV, Bookstein FL, Moreton IJ (2000) Statistical assessment of bilateral symmetry of shapes. *Biometrika*, **87**, 285–300.

© 2014 The Authors. *Molecular Ecology* Published by John Wiley & Sons Ltd.

Marie PJ, Hay E (2013) Cadherins and Wnt signalling: a functional link controlling bone formation. *BoneKEy Reports*, **2**, 330.

Masserdotti G, Badaloni A, Green YS *et al.* (2010) ZFP423 coordinates Notch and bone morphogenetic protein signaling, selectively up-regulating Hes5 gene expression. *Journal of Biological Chemistry*, **285**, 30814–30824.

Muller GB, Newman SA (2003) Origination of organismal form: The forgottten cause in evolutionary biology. In: *Origination of Organismal Form: Beyond the Gene in Developmental and Evolutionary Biology* (eds Muller GB, Newman SA), pp. 4–10. MIT Press, Cambridge, MA.

Orr HA (2005) The genetic theory of adaptation: a brief history. *Nature Reviews Genetics*, **6**, 119–127.

Pallerla SR, Pan Y, Zhang X, Esko JD, Grobe K (2007) Heparan sulfate Ndst1 gene function variably regulates multiple signaling pathways during mouse development. *Developmental Dynamics*, **236**, 556–563.

Paternoster L, Zhurov AI, Toma AM *et al.* (2012) Genome-wide association study of three-dimensional facial morphology identifies a variant in PAX3 associated with nasion position. *American Journal of Human Genetics*, **90**, 478–485.

Peters T, Ausmeier K, Dildrop R, Ruther U (2002) The mouse Fused toes (Ft) mutation is the result of a 1.6-Mb deletion including the entire Iroquois B gene cluster. *Mammalian Genome*, **13**, 186–188.

Poissant J, Davis CS, Malenfant RM, Hogg JT, Coltman DW (2012) QTL mapping for sexually dimorphic fitness-related traits in wild bighorn sheep. *Heredity*, **108**, 256–263.

Purcell S, Neale B, Todd-Brown K *et al.* (2007) PLINK: a toolset for whole-genome association and population-based linkage analysis. *American Journal of Human Genetics* **81**, 559–575.

Renaud S, Auffray JC (2010) Adaptation and plasticity in insular evolution of the house mouse mandible. *Journal of Zoological Systematics and Evolutionary Research*, **48**, 138–150.

Renaud S, Auffray JC, de la Porte S (2010) Epigenetic effects on the mouse mandible: common features and discrepancies in remodeling due to muscular dystrophy and response to food consistency. *BMC Evolutionary Biology*, **10**, 28.

Rieseberg LH, Buerkle CA (2002) Genetic mapping in hybrid zones. *The American Naturalist*, **159**(Suppl 3), S36–50.

Schielzeth H, Husby A (2014) Challenges and prospects in genome-wide quantitative trait loci mapping of standing genetic variation in natural populations. *Annals of the New York Academy of Sciences* **1320**, 35–57.

Schunke A, Bromiley P, Tautz D, Thacker N (2012) TINA manual landmarking tool: software for the precise digitization of 3D landmarks. *Frontiers in Zoology*, **9**, 6.

Shur I, Socher R, Benayahu D (2006) *In vivo* association of CReMM/CHD9 with promoters in osteogenic cells. *Journal of Cellular Physiology*, **207**, 374–378.

Siahsarvie R, Auffray J-C, Darvish J *et al.* (2012) Patterns of morphological evolution in the mandible of the house mouse *Mus musculus* (Rodentia: Muridae). *Biological Journal of the Linnean Society*, **105**, 635–647.

Slate JON (2005) Quantitative trait locus mapping in natural populations: progress, caveats and future directions. *Molecular Ecology*, **14**, 363–379.

Slate J (2013) From Beavis to beak color: a simulation study to examine how much QTL mapping can reveal about the genetic architecture of quantitative traits. *Evolution*, **67**, 1251–1262.

Slate J, Visscher PM, MacGregor S *et al.* (2002) A genome scan for quantitative trait loci in a wild population of red deer (*Cervus elaphus*). *Genetics*, **162**, 1863–1873.

Stratakis CA, Lafferty A, Taymans SE, Gafni RI, Meck JM, Blancato J (2000) Anisomastia associated with interstitial duplication of chromosome 16, mental retardation, obesity, dysmorphic facies, and digital anomalies: molecular mapping of a new syndrome by fluorescent *in situ* hybridization and microsatellites to 16q13 (D16S419-D16S503). *The Journal of Clinical Endocrinology and Metabolism*, **85**, 3396–3401.

Teeter KC, Payseur BA, Harris LW *et al.* (2008) Genome-wide patterns of gene flow across a house mouse hybrid zone. *Genome Research*, **18**, 67–76.

Turner LM, Harr B (in press) Genome-wide mapping in a house mouse hybrid zone reveals hybrid sterility loci and Dobzhansky-Muller interactions. *eLife*.

Turner LM, Schwahn DJ, Harr B (2012) Reduced male fertility is common but highly variable in form and severity in a natural house mouse hybrid zone. *Evolution*, **66**, 443–458.

Vierkotten J, Dildrop R, Peters T, Wang B, Ruther U (2007) Ftm is a novel basal body protein of cilia involved in Shh signalling. *Development*, **134**, 2569–2577.

Wilkie AOM, Morris-Kay GM (2001) Genetics of craniofacial development and malformation. *Nature Genetics*, **2**, 458–468.

Wolf JB, Leamy LJ, Routman EJ, Cheverud JM (2005) Epistatic pleiotropy and the genetic architecture of covariation within early and late-developing skull trait complexes in mice. *Genetics*, **171**, 683–694.

Yalcin B, Nicod J, Bhomra A *et al.* (2010) Commercially available outbred mice for genome-wide association studies. *PLoS Genetics* **6**, e1001085.

Yang H, Ding Y, Hutchins LN *et al.* (2009) A customized and versatile high-density genotyping array for the mouse. *Nature Methods*, **6**, 663–666.

Yang J, Benyamin B, McEvoy BP *et al.* (2010) Common SNPs explain a large proportion of the heritability for human height. *Nature Genetics*, **42**, 565–569.

Yang H, Wang JR, Didion JP *et al.* (2011a) Subspecific origin and haplotype diversity in the laboratory mouse. *Nature Genetics*, **43**, 648–655.

Yang J, Lee SH, Goddard ME, Visscher PM (2011b) GCTA: a tool for genome-wide complex trait analysis. *American Journal of Human Genetics*, **88**, 76–82.

Yang J, Manolio TA, Pasquale LR *et al.* (2011c) Genome partitioning of genetic variation for complex traits using common SNPs. *Nature Genetics*, **43**, 519–525.

Zelditch ML, Swiderski DL, Sheets HD (2012) *Geometric Morphometrics for Biologists: A Primer*. Elsevier Academic Press, USA.

Zhang S, Cagatay T, Amanai M *et al.* (2007) Viable mice with compound mutations in the Wnt/Dvl pathway antagonists nkd1 and nkd2. *Molecular and Cellular Biology*, **27**, 4454–4464.

Zhou X, Stephens M (2012) Genome-wide efficient mixed-model analysis for association studies. *Nature Genetics*, **44**, 821–824.

Zhou X, Carbonetto P, Stephens M (2013) Polygenic modeling with Bayesian sparse linear mixed models. *PLoS Genetics* **9**, e1003264.

© 2014 The Authors. *Molecular Ecology* Published by John Wiley & Sons Ltd.

L.F.P. and D.T. designed the study. B.H. and L.M.T. provided the mice and the genotypes. L.F.P. phenotyped the mice, and analyzed the data with help from B.H., L.F.P. and D.T. wrote the manuscript with input from B.H. and L.M.T. All the authors read and approved the final version of the manuscript.

Data accessibility

The phenotype data, the LD-pruned and the original SNP data, as well as kinship matrix are available at DRYAD: doi: 10.5061/dryad.bt848.

Supporting information

Additional supporting information may be found in the online version of this article.

Fig. S1 Regression of shape scores vs. percentage of *M. m. domesticus* alleles in the respective animal for the skull (a) and the mandible (b).

Fig. S2 Phenotypic effect of the significant SNPs.

Fig. S3 Distribution of the best *P*-values of 10 000 permutations for mandible and skull.

Fig. S4 QQ plots of the phenotypes (principal components) that showed significant association with the markers.

Fig. S5 Principal component axes significantly associated with genomic loci.

Fig. S6 Principal component axes significantly associated with genomic loci.

Table S1 Description of the landmarks used in skull and mandible.

Table S2 Principal components included in the mapping.

© 2014 The Authors. *Molecular Ecology* Published by John Wiley & Sons Ltd.